Direction-dependent optical solitary waves in nematic liquid crystals

Enrique Calisto [1] and Gaetano Assanto [2]
[1]*School of Mathematics, University of Edinburgh, Edinburgh EH9 3FD, Scotland, United Kingdom*
[2]*Nonlinear Optics and OptoElectronics Laboratory, Roma Tre University, 00146 Rome, Italy*

(Received 13 July 2023; accepted 4 October 2023; published 17 October 2023)

We investigate the optical propagation of reorientational solitary waves in nonuniformly oriented planar samples of thermotropic liquid crystals in the nematic phase. A nonsymmetric distribution of the optic axis, across either the longitudinal or transverse coordinates, entails nematicon paths affected by the side of the cell where the excitation is launched, i.e., direction-sensitive trajectories. We analyze the effect with reference to realistic samples encompassing a linearly modulated orientation vs either length or width, presenting nonlinear models and the outcome of numerical experiments. We briefly discuss the resulting nonspecular transmission in terms of optical nonreciprocity and isolation.

DOI: 10.1103/PhysRevA.108.043509

I. INTRODUCTION

In the past few decades, thermotropic liquid crystals in the nematic mesophase (NLCs) have been employed as an ideal anisotropic dielectric for studying various nonlinear optical phenomena related to polarization as well as intensity-dependent responses to electromagnetic wave packets at optical frequencies, including modulational instability, random lasing, spatial solitons, and shock waves [1–11]. In particular, spatial solitary waves in nematic liquid crystals, usually referred to as nematicons [12,13], are stable and robust self-confined beams which can propagate diffractionless within the light-induced channel waveguide, typically wider than the optical wave packet owing to a highly nonlocal response [14,15]. This prevents catastrophic collapse and mediates long-range interactions between nonlinear beams [16,17]. Since nematicons can be launched at milliwatt power levels from light beams in planar geometries allowing for a nematic phase, they have been the subject of several enlightening investigations, including waveguiding and collisions, bistability and hysteresis, reconfigurability and negative refraction, and voltage or magnetic steering control, to mention a few effects of interest for soliton fundamental science as well as potential applications [12,13]. In the theoretical domain, nematicons are described by nonlinear dispersive-wave equations, modeled by a nonlinear Schrödinger-like equation for the propagating envelope and an elliptic equation for the reorientational response, due to the electric-field torque applied onto the anisotropic molecular dipoles in a liquid state [18].

Nematicons in reorientational NLCs are extraordinarily polarized wave packets self-guided via the all-optical increase of the extraordinary wave refractive index. Although optical wave packets, including solitary waves, are expected to propagate straight in homogeneous isotropic dielectrics, their trajectory in highly nonlocal and birefringent liquid crystals is determined and can be controlled by the distribution of the optic axis, e.g., by introducing local or nonlocal perturbations or modulations of its angular orientation, including defects, interfaces, or lenslike regions [12,13,18]. Since the optic axis $\vec{n}$ of the equivalent uniaxial crystal corresponds to the NLC molecular director, its spatial distribution can be engineered by suitable anchoring at the confining interfaces or by the use of external means. The angular orientation of $\vec{n}$ with respect to the beam wave vector $\vec{k}$ locally determines both the index of refraction n_e and the walkoff angle δ between $\vec{k}$ and the Poynting vector $\vec{s}$ of extraordinarily polarized waves.

When considering a standard geometry, i.e., a planar NLC cell with input and output interfaces or ports for the light beam separated by a propagation distance L, the all-optical response (supporting solitary waves) in the presence of a nonsymmetric inhomogeneity or modulation (giving rise to a distribution of index and walkoff) can translate into nonspecular beam paths when identical excitations are launched from opposite sides. This direction-dependent response is one of the mechanisms exploited for passive nonlinear isolators, such as those based on degenerate three-photon interactions or Kerr directional coupling [19,20].

In this paper, inspired by the diodelike behavior of previously demonstrated nonsymmetric nonlinear optical configurations [19] and previous reports on bent nematicons in NLCs with nonuniform anchoring [21,22], we analyze the direction dependence of nematicon beams and waveguides excited in planar NLC cells with angular orientation of the optic axis being modulated along either the longitudinal or the transverse coordinate direction. We conduct numerical experiments to investigate the evolution and trajectories of solitary waves launched from opposite sides of the cell, specifically their amplitudes, profiles, and transverse separation when forward-propagating (FP) output and backward-propagating (BP) input locations coincide. We briefly discuss nonspecular transmission of self-confined and guided waves in terms of reciprocity and optical isolation.

II. MODEL

We examine geometries in planar cells of length L, width d, and thickness h ($h \ll d, L$) along the z, y, and x axes, respectively, with (x, y, z) a standard system of mutually orthogonal

Cartesian axes. We assume the positive uniaxial NLC to be prepared in the nematic mesophase with an order parameter close to unity and molecular director $\vec{n}$ oriented in the (y, z) plane, the principal plane where the electric field, wave vector $\vec{k}$, and Poynting vector $\vec{s}$ of extraordinarily polarized light lie. Here we denote by θ the orientation angle between $\vec{k}$ and $\vec{n}$ and by δ the walkoff between $\vec{s}$ and $\vec{k}$. Throughout this study, in the linear regime $\theta = \theta(y, z)$, whereas the nonlinear reorientation $\psi = \psi(x, y, z)$ induced by an extraordinarily polarized beam is a small perturbation to θ, with the overall orientation being $\Theta = \theta + \psi$ and $\psi \ll \theta$.

Nematicons stem from the robust balance between linear diffraction and a nonlinear extraordinary wave index increase $n_e = n_e[\Theta(x, y, z)] \approx n_e[\theta(y, z)] + \psi dn_e(\theta)/d\theta$ in the planar geometries of interest and in the presence of a nonlocal and saturable all-optical response. The latter gives rise to graded-index channel waveguides featuring a large numerical aperture and is able to confine extraordinarily polarized signals, with (energy flux) propagation at an angle δ with respect to the input wave vector. It is convenient to recall from the optics of uniaxial media that

$$n_e(\theta) = \frac{n_\perp n_\parallel}{[(n_\perp^2 - n_\parallel^2)\sin^2\theta + n_\parallel^2]^{1/2}}, \tag{1}$$

$$\delta(\theta) = -\frac{1}{n_e(\theta)}\frac{dn_e(\theta)}{d\theta}, \tag{2}$$

with $c_0/n_\perp$ ($c_0/n_\parallel$) the ordinary-wave (extraordinary-wave) phase-velocity eigenvalue (here c_0 denotes the speed of light in vacuum). We define the optical anisotropy $\Delta\epsilon = n_\parallel^2 - n_\perp^2$ and $\Delta = \tan\delta$ such that

$$\Delta(\Theta) = \frac{\Delta\epsilon \sin 2\Theta}{\Delta\epsilon + 2n_\perp^2 + \Delta\epsilon\cos 2\Theta}, \tag{3}$$

accounting for the nonlinear perturbation as well.

For a light beam polarized as an extraordinary wave and propagating along z, in the paraxial approximation with an injected component $E = E_y$ of the electric field and neglecting $E_z \ll E_y$, assuming transverse confinement across x in the solitary-wave regime [23], the evolution of the envelope E in the principal plane (y, z) is ruled by the nonlinear Schrödinger-type equation

$$2ik_0 n_e\left(\frac{\partial E}{\partial z} + \Delta(\Theta)\frac{\partial E}{\partial y}\right) + \frac{\partial^2 E}{\partial y^2} + k_0^2(n_\perp^2\cos^2\Theta)E + k_0^2(n_\parallel^2\sin^2\Theta - n_\perp^2\cos^2\theta_0 - n_\parallel^2\sin^2\theta_0)E = 0. \tag{4}$$

Equation (4) needs to be coupled to the NLC reorientation model, which can be obtained from the minimization of the Frank-Oseen energy density as the Euler-Lagrange equation

$$K_{22}\frac{\partial^2\Theta}{\partial x^2} + (K_{11}\cos^2\Theta + K_{33}\sin^2\Theta)\frac{\partial^2\Theta}{\partial y^2} - \frac{1}{2}\sin 2\Theta(K_{11} - K_{33})\left(\frac{\partial\Theta}{\partial y}\right)^2 + \frac{\epsilon_0\Delta\epsilon}{2}(\sin 2\Theta E^2) = 0,$$

with K_{11}, K_{22}, and K_{33} the Frank elastic constants for, respectively, splay, twist, and bend deformations in the distribution of the molecular director $\vec{n} = (0, \sin\Theta, \cos\Theta)$ in the specific $(1 + 1)$-dimensional geometry under consideration. In the single-constant approximation whereby the elastic deformations are taken to be equal, i.e., $K_{11} = K_{22} = K_{33} = K$, the Euler-Lagrange equation above can be recast as

$$K\frac{\partial^2\Theta}{\partial y^2} + \frac{1}{4}\epsilon_0\Delta\epsilon|E|^2\sin 2\Theta = 0. \tag{5}$$

The nematicon model equations (4) and (5) are hard to solve in general [24]. In the frame of the first-order perturbation theory, taking the all-optical reorientation ψ to be much smaller than the background orientation θ and expanding the trigonometric functions, Eqs. (4) and (5) reduce to

$$2ik_0 n_e\left(\frac{\partial E}{\partial z} + \Delta(\Theta)\frac{\partial E}{\partial y}\right) + \frac{\partial^2 E}{\partial y^2} + k_0^2\Delta\epsilon[\sin^2\theta - \sin^2\theta_0 + \sin(2\theta)\psi]E = 0, \tag{6}$$

$$K\frac{\partial^2\psi}{\partial y^2} + \frac{1}{4}\epsilon_0\Delta\epsilon|E|^2\sin(2\theta) = 0. \tag{7}$$

In this paper we consider the simple cases of either a purely longitudinal modulation $\theta = \theta(z)$ or a purely transverse modulation $\theta = \theta(y)$. In the former limit, using the phase transformation

$$E \to E\exp\left(\frac{ik_0}{2n_e}\int_0^z[\Delta\epsilon(\sin^2\theta - \sin^2\theta_0)]du\right), \tag{8}$$

the electric-field equation becomes

$$2ik_0 n_e\left(\frac{\partial E}{\partial z} + \Delta(\Theta)\frac{\partial E}{\partial y}\right) + \frac{\partial^2 E}{\partial y^2} + k_0^2\Delta\epsilon[\sin(2\theta)]\psi E = 0.$$

We introduce the dimensionless coordinates (Y, Z),

$$y = \frac{\lambda}{\pi\sqrt{\Delta\epsilon\sin 2\theta_0}}Y, \quad z = \frac{2n_e\lambda}{\pi\Delta\epsilon\sin 2\theta_0}Z,$$

and the unitless amplitude u of the electric-field envelope

$$E = \sqrt{\frac{4P_b}{\pi\epsilon_0 c n_e W_b^2}}u \tag{9}$$

in order to get

$$i\frac{\partial u}{\partial Z} + i\gamma\Delta(\Theta)\frac{\partial u}{\partial Y} + \frac{1}{2}\frac{\partial^2 u}{\partial Y^2} + 2\frac{\sin[2\theta(Z)]}{\sin[2\theta(0)]}\psi u = 0, \tag{10}$$

$$\nu\frac{\partial^2\psi}{\partial Y^2} + 2\frac{\sin[2\theta(Z)]}{\sin[2\theta(0)]}|u|^2 = 0, \tag{11}$$

with λ the wavelength. For this case $\theta = \theta(z)$ we also define the walkoff coefficient γ and elasticity parameter ν as

$$\gamma = \frac{2n_e}{\sqrt{\Delta\epsilon\sin[2\theta(0)]}}, \quad \nu = \frac{2\pi^3 c n_e K W_b^2}{\lambda^2 P_b}. \tag{12}$$

The nondimensionalization above is based on a reference Gaussian beam of power P_b and half-width W_b, whose values are taken as $P_b = 2.7$ mW and $W_b = 3.5$ μm, respectively, consistently with typical experimental parameters.

When $\theta = \theta(y)$, i.e., in a planar cell with orientation modulation in the transverse coordinate direction only, the electric-field transformation (8) cannot be applied and the

dimensionless model is then

$$i\frac{\partial u}{\partial Z} + i\gamma\Delta(\Theta)\frac{\partial u}{\partial Y} + \frac{1}{2}\frac{\partial^2 u}{\partial y^2} + \{\sin^2\theta(Y) - \sin^2\theta_0 + \sin[2\theta(Y)]\psi\}u = 0, \quad (13)$$

$$\nu\frac{\partial^2\psi}{\partial Y^2} + 2\{\sin[2\theta(Y)]\}|u|^2 = 0. \quad (14)$$

Here, at variance with Eq. (12),

$$\nu = \frac{2\pi^3 c n_e K W_b^2}{\lambda^2 P_b}, \quad \gamma = \frac{2n_e}{\sqrt{\Delta\epsilon}}. \quad (15)$$

In the numerical experiments we adopt material parameters typical of the NLC mixture E7, with $n_\parallel = 1.7$, $n_\perp = 1.5$, and $K = 1.2 \times 10^{-11}$ N, with elasticity or nonlocality parameter $\nu = 250$. We consider a planar cell of size $(h, d, L) = (30, 600, 1000)$ μm and Gaussian beams of wavelength 1064 nm in the extraordinary polarization launched forward in $(y_0, 0)$ or backward in $(y_{FP}(L), L)$, with $y_{FP}(L)$ the transverse position of the outgoing FP wave packet. The electric-field equation is solved in Y using the fast Fourier transform and propagated in Z using a fourth-order Runge-Kutta scheme.

III. LINEAR LONGITUDINAL MODULATION

First, we consider a planar cell where the background orientation (at rest) has a linear dependence across the length L of the NLC sample and is uniform across the width, with $\theta_0 = \theta(z = 0)$ and $\theta_L = \theta(z = L)$. As in a preliminary report [22], we launch identical input beams with $\vec{k} = \vec{z}$ for forward propagation and $\vec{k} = -\vec{z}$ for backward propagation, using the reference values of beam power, width, and wavelength to ensure the formation and propagation of nematicons throughout this study. For a linear variation from $\theta_0 = 10^\circ$ to $\theta_L = 45^\circ$, Fig. 1(a) displays the refractive index $n_e(z)$ and walkoff $\delta(z)$ distributions in the cell, whereas Figs. 1(b)–1(d) graph the resulting FP and BP nematicon transverse profiles (input, FP output, and BP output), their amplitude evolution (linked to their width via the transverse profile as ideal nematicons conserve power) and trajectories versus z, respectively. It is apparent that, owing to the nonlinear response in the absence of midcell symmetry, the z-modulated responses in nonlinearity and walkoff result in distinct evolution of the FP wave packet compared to the BP wave packet, with the BP output location well separated from the FP input $y = 0$ and $\Delta y = y_{BP}(0) - y_{FP}(0) \approx 50$ μm, well in excess of the nematicon spot size. Figures 2(a)–2(d) illustrate the case of modulation from $\theta_0 = 20^\circ$ to $\theta_L = 60^\circ$, with $\Delta y \approx 40$ μm. Finally, while the transverse separation Δy is zero in the linear limit ($\psi = 0$), it is a function of the input power in the reorientational regime, as plotted in Figs. 3(a) and 3(b) for two different intervals of linearly varying orientation $\theta(z)$.

IV. LINEAR TRANSVERSE MODULATION

While in the preceding section nematicons launched from opposite sides of the samples underwent different (linear as well as power-dependent) walkoff, in an NLC sample with orientation modulation in the transverse coordinate y direction, both walkoff and refraction act on the wave packets, as they propagate through regions with modulated refraction. Figures 4(a)–4(d) show the refractive index $n_e(y)$ and walkoff $\delta(y)$ distributions in a y-modulated cell with orientation linearly modulated from $\theta_{bot} = 65^\circ$ to $\theta_{top} = 25^\circ$ across the width d and an FP input launched in $(y_0, z) = (100$ μm, 0)

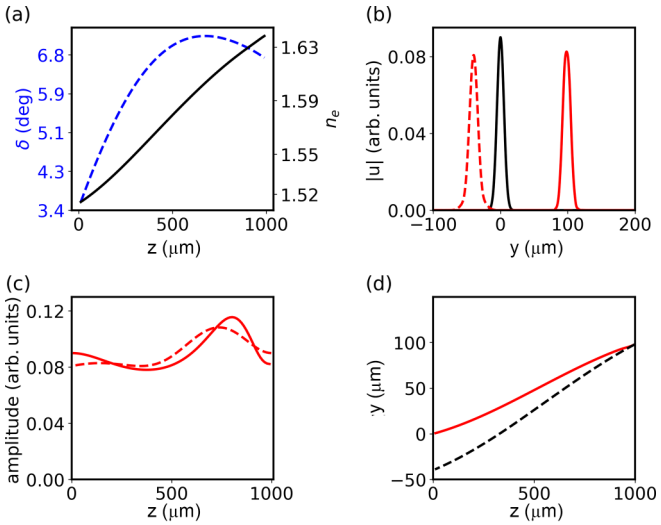

FIG. 1. Linear longitudinal modulation from $\theta_0 = 10^\circ$ to $\theta_L = 45^\circ$. (a) Refractive index $n_e(z)$ (black solid line) and angular walkoff $\delta(z)$ (blue dashed line) versus z in a 1-mm-long cell filled with E7. (b) Transverse profiles of input (black solid line), FP transmitted (red solid line), and BP transmitted (red dashed line) wave packets. (c) Amplitudes of FP (solid line) and BP (dashed line) nematicons versus z. (d) Trajectories of FP (solid line) and BP (dashed line) nematicons in the (y, z) plane.

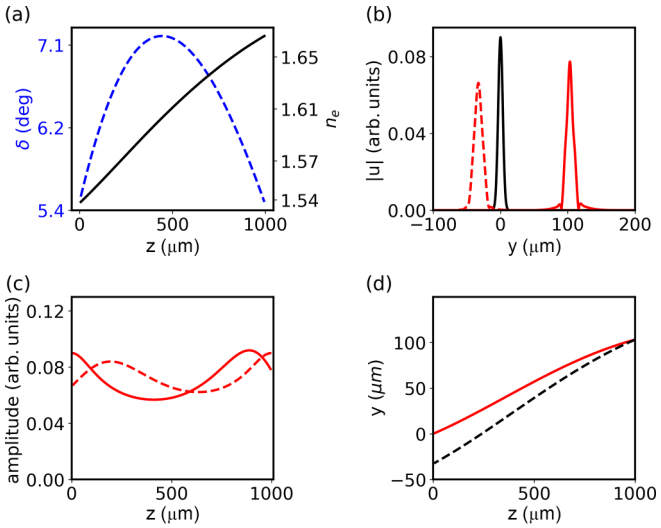

FIG. 2. Linear longitudinal modulation from $\theta_0 = 20^\circ$ to $\theta_L = 60^\circ$. (a) Refractive index $n_e(z)$ (black solid line) and walkoff $\delta(z)$ (blue dashed line) distributions. (b) Profiles of input, FP output, and BP output. (c) Amplitudes of FP (solid line) and BP (dashes) solitons versus propagation. (d) Trajectories of FP (red solid line) and BP (black dashed line) nematicons.

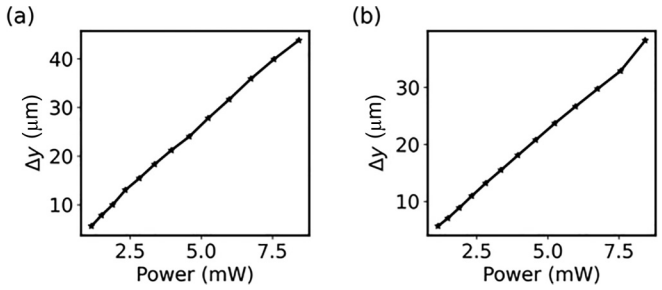

FIG. 3. Linear longitudinal modulation. The beam power dependence of transverse separation Δy is plotted for (a) $\theta_0 = 10^\circ$ to $\theta_L = 45^\circ$ and (b) $\theta_0 = 20^\circ$ to $\theta_L = 60^\circ$. Dots are calculated points and lines are guides to the eye.

with $\theta(y_0) = 38^\circ$. In this case (see also Ref. [21]) refraction and walkoff tend to counteract their effects on the FP beam, whereas they act synergistically on the BP wave packet, with a resulting $\Delta y \approx -180$ μm. Figures 5(a)–5(d) display another case, where the orientation goes from $\theta_{\rm bot} = 25^\circ$ to $\theta_{\rm top} = 65^\circ$ and the FP beam is launched in $(y_0, z) = (-200\ \mu{\rm m}, 0)$ with $\theta(y_0) = 32^\circ$ and $\Delta y \approx 180$ μm. Figures 6(a) and 6(b) illustrate the corresponding power dependence of Δy.

V. DISCUSSION

The simple layout we examined here can be regarded as a two-port guided-wave device, in which forward and backward extraordinarily polarized signals are confined in the nematicon waveguides excited by counterpropagating beams of equal powers and profiles. In this respect, since the BP output signal (nematicon) is not superposed with the FP input signal (nematicon), these NLC cells could be regarded as optical isolators or diodes, with low signal crosstalk and high rejection depending on the separation ($\Delta y \gg W_b$) and adjustable with power and/or orientation modulation. Since the phenomenon rests essentially on the nonspecular distribution θ of the optic axis with respect to input and output ports, the description of the NLC samples in terms of a dielectric stack would result in an asymmetric dielectric tensor [25]. Moreover, the self-focusing response associated with reorientation is at the origin of nematicon formation and soliton waveguides. Hence, according to Potton [26] and de Hoop [27], the previous considerations support the claim of a nonreciprocal transmission despite the passive and nonmagnetic character of the (undoped) nematic liquid crystals. While reciprocity and nonreciprocity are more often addressed in

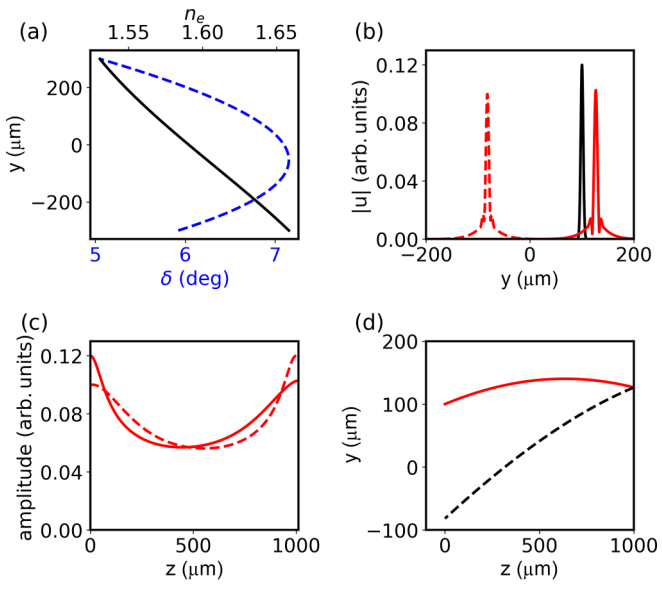

FIG. 4. Linear transverse modulation from $\theta_{\rm bot} = 65^\circ$ to $\theta_{\rm top} = 25^\circ$ across a cell width $d = 600$ μm. (a) Refractive index $n_e(y)$ (black solid line) and angular walkoff $\delta(y)$ (blue dashed line) in a 1-mm-long cell. (b) Transverse profiles of input (black solid line), FP output (red solid line), and BP output (red dashed line) wave packets. (c) Amplitudes of FP (solid line) and BP (dashed line) nematicons. (d) Trajectories of FP (red solid line) and BP (black dashed line) nematicons.

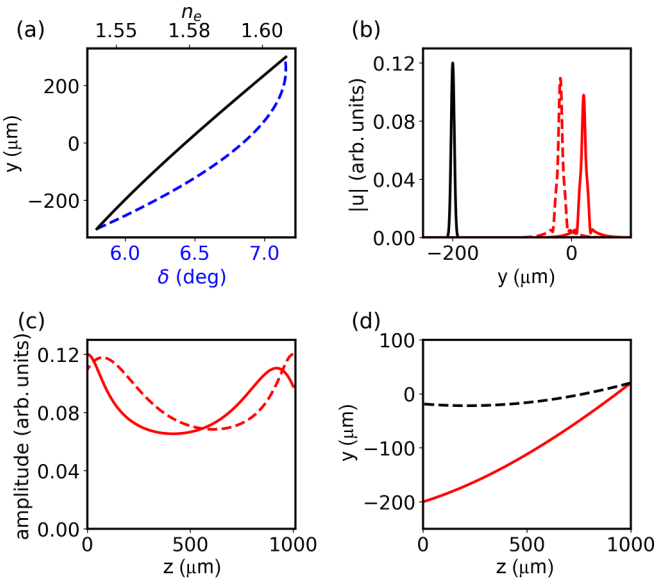

FIG. 5. Linear transverse modulation from $\theta_{\rm bot} = 25^\circ$ to $\theta_{\rm top} = 65^\circ$ across $d = 600$ μm. (a) Refractive index $n_e(y)$ (black solid line) and angular walkoff $\delta(y)$ (blue dashed line). (b) Transverse profiles of input (black solid line), FP output (red solid line), and BP output (red dashed line). (c) Amplitudes of FP (solid line) and BP (dashed line) nematicons. (d) Trajectories of FP (red solid line) and BP (black dashed line) nematicons.

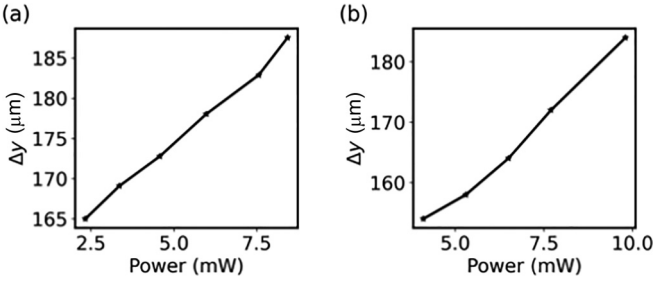

FIG. 6. Linear transverse modulation. The beam power dependence of transverse separation Δy is plotted for (a) $\theta_{\rm bot} = 25^\circ$ to $\theta_{\rm top} = 65^\circ$ and (b) $\theta_{\rm bot} = 65^\circ$ to $\theta_{\rm top} = 25^\circ$. Dots are calculated points and lines are guides to the eye.

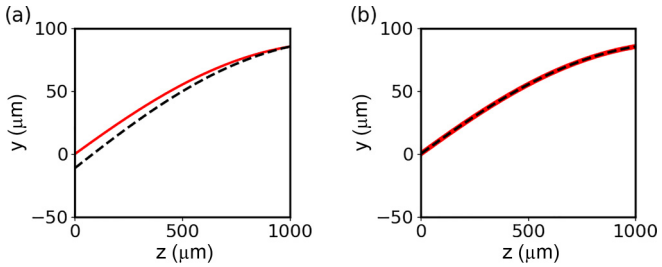

FIG. 7. Linear longitudinal modulation in a sample with $\theta_0 = 45^\circ$ and $\theta_L = 70^\circ$. The FP (red solid line) and BP (black dashed line) trajectories are plotted for (a) identical counterlaunched input beams and (b) phase-conjugated reflection. The BP input is phase conjugated with respect to the FP output.

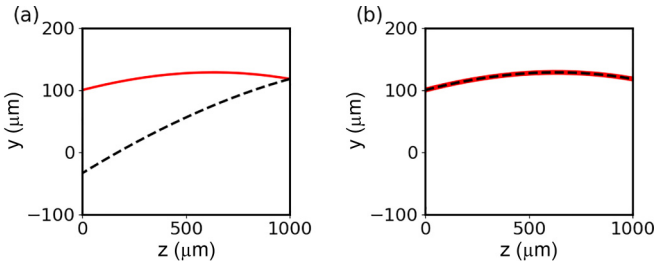

FIG. 8. Linear transverse modulation in a cell with $\theta_{\text{bot}} = 75^\circ$ and $\theta_{\text{top}} = 45^\circ$. The FP (red solid line) and BP (black dashed line) trajectories are plotted for (a) identical counterlaunched input beams and (b) phase-conjugated reflection.

the absence of confinement and nonlinear effects, the effect described herein does not belong to the class of those scattering configurations where inverting the sign of wave vectors and exchanging source(s) and detector(s) leads to the same transmission, qualifying them as reciprocal [25]. Nevertheless, reciprocity and time reversal are often used interchangeably; to verify whether the modulated NLC samples satisfy time reversibility, we repeated the numerical experiments above in the limit of phase-conjugated reflection, i.e., using for the BP input the FP output after phase conjugation. The results, shown in two instances of z- and y-modulated orientation in Figs. 7 and 8, respectively, demonstrate that, albeit seemingly nonreciprocal, what we reported is actually time reversible. Finally, in terms of potential applications of nonreciprocal systems to isolation, the studied configurations lend themselves to optical isolators as qualified by Jalas *et al.* in Ref. [28]. The confinement of copolarized signals afforded by reorientational solitary waves in NLC allows the device defined by the two ports in $(y_{\text{FP}}(0), 0)$ and $(y_{\text{FP}}(L), L)$ to operate as a (nonlinear) optical diode, which transmits forward to port 2 $(y_{\text{FP}}(L), L)$ only FP signals injected in port 1 $(y_{\text{FP}}(0), 0)$ while isolating port 1 from signals launched in port 2. Moreover, this diodelike operation, consistently with the use of guided signals, would not be affected by dynamic reciprocity [29].

VI. CONCLUSION

We addressed the formation and propagation of optical spatial solitons in orientation-modulated nematic liquid crystals, nematicons, outlining their direction-sensitive evolutions and trajectories when launched from opposite sides of nonspecular samples. The reported layout is time reversible but, owing to nonlinear and asymmetric dielectric responses, lacks reciprocity and yields optical isolation between counterpropagating signals copolarized with and confined by nematicons. Simple linear variations of the background orientation of the molecular director were presented and discussed using a simplified $(1 + 1)$-dimensional model; $(2 + 1)$-dimensional propagation and more complex functional forms of orientation modulation are left for future consideration.

ACKNOWLEDGMENTS

E.C. acknowledges financial support from ANID (Chile) through Beca Doctorado Extranjero (Grant No. 72210165). This material is based upon work supported by the Air Force Office of Scientific Research (USA) under Award No. FA8655-23-1-7026.

[1] I. C. Khoo, Nonlinear optics of liquid crystalline materials, Phys. Rep. **471**, 221 (2009).
[2] A. E. Miroshnichenko, E. Brasselet, and Y. S. Kivshar, Light-induced orientational effects in periodic photonic structures with pure and dye-doped nematic liquid crystal defects, Phys. Rev. A **78**, 053823 (2008).
[3] J. Beeckman, X. Hutsebaut, M. Haelterman, and K. Neyts, Induced modulation instability and recurrence in nematic liquid crystals, Opt. Express **15**, 11185 (2007).
[4] G. Strangi, S. Ferjani, V. Barna, A. De Luca, N. Scaramuzza, C. Versace, C. Umeton, and R. Bartolino, Random lasing and weak localization of light in dye-doped nematic liquid crystals, Opt. Express **14**, 7737 (2006).
[5] M. A. Karpierz, Solitary waves in liquid crystalline waveguides, Phys. Rev. E **66**, 036603 (2002).
[6] M. Peccianti and G. Assanto, Nematic liquid crystals: A suitable medium for self-confinement of coherent and incoherent light, Phys. Rev. E **65**, 035603(R) (2002).
[7] M. Warenghem, J. F. Blach, and J. F. Henninot, Thermonematicon: An unnatural coexistence of solitons in liquid crystals? J. Opt. Soc. Am. B **25**, 1882 (2008).
[8] A. Ramaniuk, P. S. Jung, D. N. Christodoulides, W. Krolikowski, and M. Trippenbach, Absorption-mediated stabilization of nonlinear propagation of vortex beams in nematic liquid crystals, Opt. Commun. **451**, 338 (2019).
[9] S. Perumbilavil, A. Piccardi, R. Barboza, O. Buchnev, G. Strangi, M. Kauranen, and G. Assanto, Beaming random lasers with soliton control, Nat. Commun. **9**, 3863 (2018).
[10] G. Assanto and N. F. Smyth, Spin-optical solitons in liquid crystals, Phys. Rev. A **102**, 033501 (2020).

[11] S. Baqer, D. J. Frantzeskakis, T. P. Horikis, C. Houdeville, T. R. Marchant, and N. F. Smyth, Nematic dispersive shock waves from nonlocal to local, Appl. Sci. **11**, 4736 (2021).
[12] M. Peccianti and G. Assanto, Nematicons, Phys. Rep. **516**, 147 (2012).
[13] G. Assanto, Nematicons: Reorientational solitons from optics to photonics, Liq. Cryst. Rev. **6**, 170 (2018).
[14] C. Conti, M. Peccianti, and G. Assanto, Route to nonlocality and observation of accessible solitons, Phys. Rev. Lett. **91**, 073901 (2003).
[15] C. Conti, M. Peccianti, and G. Assanto, Observation of optical spatial solitons in a highly nonlocal medium, Phys. Rev. Lett. **92**, 113902 (2004).
[16] O. Bang, W. Krolikowski, J. Wyller, and J. J. Rasmussen, Collapse arrest and soliton stabilization in nonlocal nonlinear media, Phys. Rev. E **66**, 046619 (2002).
[17] M. Peccianti, A. Fratalocchi, and G. Assanto, Transverse dynamics of nematicons, Opt. Express. **12**, 6524 (2004).
[18] G. Assanto and N. F. Smyth, Self-confined light waves in nematic liquid crystals, Physica D **402**, 132182 (2020).
[19] K. Gallo, G. Assanto, K. R. Parameswaran, and M. M. Fejer, All-optical diode in a periodically-poled lithium niobate waveguide, Appl. Phys. Lett. **79**, 314 (2001).
[20] A. Alberucci and G. Assanto, All-optical isolation by directional coupling, Opt. Lett. **33**, 1641 (2008).
[21] U. Laudyn, M. Kwasny, F. Sala, M. Karpierz, N. F. Smyth, and G. Assanto, Curved solitons subject to transverse acceleration in reorientational soft matter, Sci. Rep. **7**, 12385 (2017).
[22] E. Calisto, N. F. Smyth, and G. Assanto, Optical isolation via direction-dependent soliton routing in birefringent soft-matter, Opt. Lett. **47**, 2782 (2022).
[23] A. Alberucci and G. Assanto, Nematicons beyond the perturbative regime, Opt. Lett. **35**, 2520 (2010).
[24] J. M. L. MacNeil, N. F. Smyth, and G. Assanto, Exact and approximate solutions for optical solitary waves in nematic liquid crystals, Physica D **284**, 1 (2014).
[25] M. Born and E. Wolf, *Principles of Optics*, 7th ed. (Cambridge University Press, Cambridge, 1999).
[26] R. J. Potton, Reciprocity in optics, Rep. Prog. Phys. **67**, 717 (2004).
[27] A. T. de Hoop, A reciprocity theorem for the electromagnetic field scattered by an obstacle, Appl. Sci. Res. **8**, 135 (1960).
[28] D. Jalas *et al.*, What is—and what is not—an optical isolator, Nat. Photon **7**, 579 (2013).
[29] Y. Shi, Z. Yu, and S. Fan, Limitations of nonlinear optical isolators due to dynamic reciprocity, Nat. Photon **9**, 388 (2015).